JOURNAL OF SPACECRAFT AND ROCKETS
Vol. 47, No. 4, July–August 2010

Aerocapture Ballutes Versus Aerocapture Tethers for Exploration of the Solar System

Kristin L. Gates* and James M. Longuski†
Purdue University, West Lafayette, Indiana 47907-2045

DOI: 10.2514/1.46603

Previous literature indicates that aerocapture with ballutes may provide significant mass advantages over traditional propulsive orbit capture. The possibility of using ballutes in the exploration of the atmosphere-bearing bodies in the solar system is considered, including Venus, Earth, Mars, Jupiter, Saturn, Titan, Uranus, and Neptune. The mass cost of ballute aerocapture is compared with propulsive capture and with previous work in which tethers are used for aerocapture in solar system exploration. Although both ballute and tether technologies require further analysis in the areas of structures, materials, and guidance, both systems offer attractive advantages over aerocapture with aeroshells and over propulsive capture.

Nomenclature

A	=	cross-sectional area, m^2
C	=	stagnation-point heating coefficient, $kg^{1/2}/m$
C_D	=	drag coefficient
d	=	tether diameter, m
e	=	eccentricity
F_T	=	tension force on the tether, N
g	=	standard acceleration of free fall, 9.80665 m/s^2
H	=	atmospheric scale height, km
I_{sp}	=	specific impulse, s
l	=	tether length, m
m	=	mass, kg
Q	=	stagnation-point heating rate, W/cm^2
R	=	radius of the atmosphere, km
R_n	=	nose radius, m
R_{sball}	=	radius of spherical ballute, m
R_{tball}	=	torus ring radius, m
r	=	radial distance, km
r_{peri}	=	radial distance at orbit periapsis, km
r_{tball}	=	torus tube radius, m
S	=	surface area, m^2
T	=	temperature, K
V	=	speed, km/s
V_{esc}	=	escape velocity, km/s
V_{peri}	=	velocity at periapsis, km/s
$V_{\infty-}$	=	approach hyperbolic excess velocity, km/s
$V_{\infty+}$	=	departure hyperbolic excess velocity, km/s
α	=	pump angle, deg
β	=	ballistic coefficient, kg/m^2
γ	=	flight-path angle, deg
Δm	=	propellant mass, kg
ΔV_{cap}	=	velocity change for orbit capture, km/s
δ	=	flyby bending angle, deg
ε	=	material emissivity
μ	=	gravitational parameter, km^3/s^2
ρ	=	atmospheric density, kg/m^3
ρ_t	=	tether material density, kg/m^3
σ	=	Stefan–Boltzmann constant, 5.67×10^{-8} $W/(m^2K^4)$
σ_{ball}	=	ballute areal density, kg/m^2
σ_u	=	ultimate strength per unit area, N/m

Subscripts

ball	=	ballute
o	=	orbiter
p	=	probe
peri	=	periapsis
ref	=	reference
sball	=	spherical ballute
t	=	tether
tball	=	toroidal ballute

Received 3 August 2009; revision received 6 April 2010; accepted for publication 8 April 2010.

*Doctoral Candidate, School of Aeronautics and Astronautics; currently Senior Engineer, Global Aerospace Corporation, 711 West Woodbury Road, Suite H, Altadena, CA 91001-5327. Student Member AIAA.

†Professor, School of Aeronautics and Astronautics, 701 West Stadium Avenue. Associate Fellow AIAA.

I. Introduction

THE concept of using a ballute for aerocapture (Fig. 1) at planets and moons with atmospheres was pioneered about a decade ago by McRonald [1–3]. Before that, inflatable drag devices were considered for sounding rockets [4], Viking lander [5], and aero-assisted orbital transfer vehicles [6]. Those early ballutes were to be deployed at low altitudes and had limited potential to affect trajectory and reduce heating. The new idea suggested by McRonald [1] is to use a large cross-sectional area ballute at high altitudes in order to decrease heating rates to levels that can be radiated without ablation at surface temperatures on the order of 500°C. Two candidate materials that can withstand such temperatures, while having enough strength, are Kapton® for ballute and polyboxoxazole (PBO) for tubing and tethers. Both Kapton and PBO are lightweight, with densities of less than 20 g/m^2 [1] (about four times lighter than one page of typical office paper) and with strength above 5600 psi. Trajectory simulations for aerocapture ballutes made of Kapton and PBO estimate that heat-shield mass may be reduced by about a factor of 2 compared to rigid aeroshells [1]. Further trajectory analysis has been conducted to investigate ballute aerocapture at multiple destinations, including Venus, Earth, Mars, Saturn, Titan, and Neptune [7–14]. Several years ago, under NASA's In-Space Propulsion program, Ball Aerospace in collaboration with the Jet Propulsion Laboratory and NASA Langley Research Center led an interdisciplinary investigation [15–17] for characterizing and refining the use of ballutes for aerocapture and in 2007, Rohrschneider and Braun [18] published a comprehensive survey of current ballute technology facilitating aerocapture.

Tethered aerocapture [19–21] is another method that allows the vehicle to remain high in the atmosphere during capture (Fig. 2). Previous work by Longuski et al. [20] compares the mass savings of tethered capture to pure propulsive capture, finding that the required tether mass is less than the required propellant mass for all cases

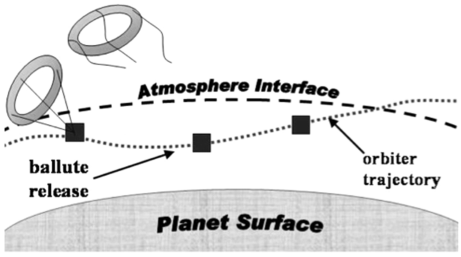

Fig. 1 Ballute aerocapture: the orbiter velocity decreases until capture into the desired orbit is achieved, at which time the ballute is released.

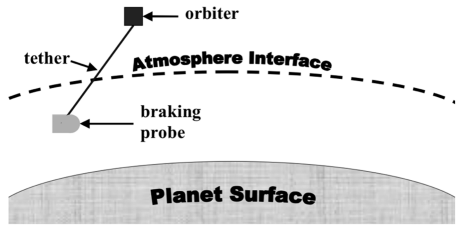

Fig. 2 Tethered aerocapture: the orbiter is attached to a heat-shielded braking probe until the desired orbit is achieved.

examined (for parabolic capture at Venus, Earth, Mars, Jupiter, Saturn, Titan, Uranus, and Neptune). We take the assessment a step further and compare the ballute mass required for parabolic capture to the results of the tether versus propellant study. In the tethered system graphite is used because of its high strength and thermal resistance. Hercules AS4 graphite, which has a tensile strength of 3.6 GN/m^2 and a density of 1800 kg/m^3, is chosen as representative of the type of material that could be used for the tether. We choose Kapton for the ballute material with a thickness of 7 μm, corresponding to an areal density of 9.94 g/m^2 and an emissivity of 0.5. Ballute simulations are conducted using the Hypersonic Planetary Aeroassist Simulation System (HyperPASS) [22], assuming a point-mass vehicle representation, a nonrotating planet, and a locally exponential atmosphere model.

The current study compares the masses of the ballute, tether, and propellant required to capture into parabolic orbit, assuming a Hohmann transfer from Earth, at each planetary destination. In the case of Earth capture, the second leg of the transfer ellipse from the Earth to Mars mission is used. The Titan mission assumes braking at Titan to get captured into orbit about Saturn. The goal of this study is to provide a baseline mass comparison of the three capture strategies and identify which planets are most suitable for ballute aerocapture. The results could influence where more studies should be done and will indicate when ballute aerocapture is favorable over propellant and tethered capture.

II. Comparative Study Specifications

We base our comparison on the masses of the propellant, ballute (both spherical and toroidal), or tether required to achieve parabolic capture at each body. For each case, the orbiter has an assumed mass of 1000 kg (a value arbitrarily chosen by Longuski et al. [20], but reflects typical values for spacecraft used in the exploration of the solar system).

The rocket equation provides the propellant mass needed to capture the orbiter into orbit ($e < 1$):

$$\Delta m = m_o[\exp(\Delta V_{\text{cap}}/I_{\text{sp}}g) - 1] \tag{1}$$

An I_{sp} of 300 s is assumed and the standard free-fall acceleration on Earth is 9.80665 m/s^2.

In the aerocapture tether, the orbiter is kept as high above the atmosphere as possible during the maneuver to avoid the need for aerodynamic shielding. The fact that the drag forces act mostly on the lower portion of the tether results in a large torque that tends to rotate the system and could easily plunge the orbiter into the atmosphere. Previous research [19] found that this could be prevented by giving the system an opposite spin rate before impact with the atmosphere. After the impact the spin rate can be eliminated to minimize tension due to centripetal forces, the exit spin rate should be opposite but equal magnitudes to the entry spin rate. When the spin rates are matched, the tension on the tether can be expressed explicitly as a function of ΔV_{cap}:

$$F_T = m_o(m_o + m_p)\Delta V_{\text{cap}}^2/(4m_p l) \tag{2}$$

The tether diameter is now determined as a function of the strength of the material chosen, since it should be designed to withstand the tension given in Eq. (2). The expression relating tether diameter to ΔV_{cap} is

$$d^2 = m_o(m_o + m_p)\Delta V_{\text{cap}}^2/(\pi m_p \sigma_u l) \tag{3}$$

The total mass of the tether [20] is

$$m_t = \rho_t m_o(m_o + m_p)\Delta V_{\text{cap}}^2/(4m_p\sigma_u) \tag{4}$$

We note that the length of the tether is not contained in the tether mass expression. That is, the mass of the tether depends only on the value of ΔV_{cap}, the masses of the orbiter and the braking probe (both 1000 kg), and the properties of the tether material, σ_u and ρ_t. Thus, from Eq. (4), we see that for a given material, the mass of the tether is not affected by its length. The reason for this is that for a given ΔV_{cap}, as the tether length is increased the tension (due to centripetal acceleration) decreases proportionally with l^{-1}, whereas the mass increases with l, so the two effects cancel.

We determine the mass of the ballute according to the ballute area required to keep the stagnation-point heating rate below the constraint. The ballute mass is added to the 1000 kg orbiter in an iterative process (described further in Sec. III). The heating rates are computed by

$$Q = CV^3\sqrt{\rho/R_n} \tag{5}$$

similar to the Sutton–Graves heating expression [23], where $R_n = R_{\text{sball}}$ for spherical ballutes and $R_n = r_{\text{tball}}$ for toroidal ballutes. The values used for the stagnation-point heating coefficient, C, to obtain Q in W/cm^2, vary with atmosphere composition and ballute shape [23,24] and are given in Table 1.

Table 1 Selected atmospheric properties[a]

Body	Composition	H, km	r_{ref}, km	ρ_{ref}, kg/m^3	C, kg$^{1/2}$/m (sphere)	C, kg$^{1/2}$/m (torus)
Venus	0.965 CO_2, 0.035 N_2	6	6150	1.0×10^{-4}	1.5740×10^{-8}	1.0650×10^{-8}
Earth	0.79 N_2, 0.20 O_2. 0.01 Ar	5	6458	7.7×10^{-6}	2.8490×10^{-8}	1.9653×10^{-8}
Mars	0.957 CO_2, 0.027 N_2. 0.016 Ar	8	3507	5.5×10^{-8}	2.6220×10^{-8}	1.9027×10^{-8}
Jupiter	0.89 H_2, 0.11 He	20	71,592	1.85×10^{-3}	0.7574×10^{-8}	0.5532×10^{-8}
Saturn	0.94 H_2, 0.06 He	30	60,350	2.8×10^{-2}	0.8613×10^{-8}	0.5371×10^{-8}
Titan	0.90 N_2, 0.10 CH_4	45	2738	1.7×10^{-3}	2.6830×10^{-8}	1.8506×10^{-8}
Uranus	0.85 H_2, 0.15 He	40	26,145	4.69×10^{-1}	0.7703×10^{-8}	0.5626×10^{-8}
Neptune	0.85 H_2, 0.15 He	40	24,750	5.76×10^{-1}	0.7703×10^{-8}	0.5626×10^{-8}

[a]The first five columns of this table are from Longuski et al. [20].

We choose two ballutes at each of the seven planets and Titan, based on a conservative maximum stagnation-point heating rate of 2 W/cm^2 for both spherical and toroidal ballute configurations. The heating rate constraint of 2 W/cm^2 is determined using the Stefan–Boltzmann radiative equilibrium equation:

$$T^4 = Q/(2\sigma\varepsilon) \tag{6}$$

where $T = 773.15$ K (or $T = 500$°C) is the surface temperature limit of the assumed ballute material Kapton, σ is 5.67×10^{-8} W/(m^{2}K^4), and $\varepsilon = 0.5$ is assumed for Kapton with a thickness of 7 μm.

We determine the ballistic coefficient β needed to achieve the required ΔV_{cap} within the heating constraints. We perform the ballute aerocapture simulations in HyperPASS, which assumes point-mass vehicle representation, inverse-square gravity field, spherical planetary bodies, and constant drag coefficient. The dimensions and masses of both spherical- and toroidal-shaped ballutes are then determined. Details on the numerical modeling are provided in the next section.

At this stage, the relative masses of the equipment involved will be ignored, such as tanks and nozzles in the propulsive system, reel and deployment equipment in the tethered system, and deployment and separation mechanisms in the ballute system. The mass of the ballute inflation gas is also considered negligible (for instance, a ballute with a volume of 11,000 m^3 and a pressure of 100 Pa will require only about 0. 67 kg of helium gas for inflation).

III. Ballute Design Considerations

We determine the size of the spherical ballute by solving for its radius R_{sball}:

$$\beta = (m_o + m_{\text{ball}})/(C_D A_{\text{ball}}) = (m_o + \sigma_{\text{ball}} S_{\text{ball}})/(C_D A_{\text{ball}}) \tag{7}$$

where

$$A_{\text{ball}} = A_{\text{sball}} = \pi R_{\text{sball}}^2, \qquad S_{\text{ball}} = S_{\text{sball}} = 4\pi R_{\text{sball}}^2 \tag{8}$$

We assume a C_D of 1 for the (ideal) hypersonic spherical ballute in each case [25].

Previous studies of toroidal ballutes were conducted for Earth returns and Titan missions by Moss [26] and Gnoffo et al. [27]. Moss [26] finds that a 4:1 (i.e., torus ring radius to torus tube radius) configuration allows the spacecraft's wake to pass through the torus' ring without disturbing the flow around the ballute. Because of this favorable result, we use a 4:1 ratio for our toroidal ballute configurations (i.e., $r_{\text{tball}} = R_{\text{tball}}/4$). Following this assumption, the ballute cross-sectional area A_{tball}, and the ballute surface area S_{tball} are used in Eq. (7) to compute the size of the toroidal ballute:

$$A_{\text{ball}} = A_{\text{tball}} = \pi R_{\text{tball}}^2, \qquad S_{\text{ball}} = S_{\text{tball}} = \pi^2 R_{\text{tball}}^2 \tag{9}$$

We assume a C_D of 1.37 for the toroidal ballute in each case [10–12].

The method of converting ΔV_{cap} values to heating rates and ballute sizes is as follows. A ballistic coefficient for the spacecraft-ballute system is picked and the mass and nose radius of the corresponding ballute (spherical or toroidal) is computed. HyperPASS simulations are then iterated to find the entry flight-path angle that results in the desired exit speed. The ballute nose radius and trajectory data can then be used to determine the maximum stagnation-point heat flux using Eq. (5). The maximum heat flux is plotted against the ballistic coefficient, and the process is repeated for other values of ballistic coefficient, resulting in a curve of maximum heat flux versus ballistic coefficient (or ballute size). The heat flux curves are then interpolated to determine the ballute size required to capture while meeting the heating constraint at each planet.

IV. Interplanetary Missions

We now consider missions at Venus, Earth, Mars, Jupiter, Saturn, Titan, Uranus, and Neptune, for which we assume a locally exponential atmosphere given by

$$\rho = \rho_{\text{ref}} \exp[-(r - r_{\text{ref}})/H] \tag{10}$$

Table 1 shows the atmospheric properties (composition, H, r_{ref}, and ρ_{ref}) assumed at each planetary body according to Longuski et al. [20].

The missions to the various planets are determined by assuming a Hohmann transfer from a 200 km Earth parking orbit. The return mission from Mars to Earth consists of the second leg of the transfer ellipse from the Earth to Mars mission. All the planets are assumed to have coplanar circular orbits about the sun, with the semimajor axes used as the orbital radii. Using a patched-conic solution, we calculate the minimum ΔV needed to capture from an incoming hyperbolic trajectory into a nearly parabolic orbit:

$$\Delta V_{\text{cap}} = \sqrt{(2\mu/r_{\text{peri}}) + V_{\infty-}^2} - \sqrt{2\mu/r_{\text{peri}}} \tag{11}$$

where μ is the planet's gravitational parameter and r_{peri} is the periapsis radius and where nearly-parabolic-capture orbit means a highly elliptic orbit with $e \to 1$.

The mission to Titan assumes braking at Titan in order to achieve capture at Saturn. We will choose the flight-path angle γ that minimizes the required aerocapture ΔV_{cap} at Titan. The hyperbolic approach velocity at Titan, $V_{\infty-,\text{titan}}$, is expressed (using the law of cosines and depicted in Fig. 3) as a function of Titan's velocity about Saturn, V_{titan}, the approach velocity at Saturn at the altitude of Titan's orbit, $V_{r(\text{titan}),\text{saturn}}$, and the flight-path angle γ:

$$V_{\infty-,\text{titan}}^2 = V_{\text{titan}}^2 + V_{r(\text{titan}),\text{saturn}}^2 - 2V_{\text{titan}} V_{r(\text{titan}),\text{saturn}} \cos(\gamma) \tag{12}$$

where

$$V_{r(\text{titan}),\text{saturn}} = \sqrt{(2\mu_{\text{saturn}}/r_{\text{saturn}\to\text{titan}}) + V_{\infty-,\text{saturn}}^2} \tag{13}$$

and

$$V_{\text{titan}} = \sqrt{\mu_{\text{saturn}}/r_{\text{saturn}\to\text{titan}}} \tag{14}$$

The required departure velocity at Titan, $V_{\infty+,\text{titan}}$ (depicted in Fig. 4), is found by solving

$$V_{\text{esc}/r(\text{titan}),\text{saturn}}^2 = V_{\text{titan}}^2 + V_{\infty+,\text{titan}}^2 - 2V_{\text{titan}} V_{\infty+,\text{titan}} \cos[\pi - (\alpha + \delta_1/2 + \delta_2/2)] \tag{15}$$

where Saturn's escape velocity at the altitude of Titan's orbit is given by

$$V_{\text{esc}/r(\text{titan}),\text{saturn}} = \sqrt{2\mu_{\text{saturn}}/r_{\text{saturn}\to\text{titan}}} \tag{16}$$

and the total rotation angle of the required departure velocity at Titan, $V_{\infty+,\text{titan}}$, is the sum of α (defined in Fig. 3) and the two half-turn angles, $\delta_1/2$ and $\delta_2/2$ (depicted in Fig. 5), where

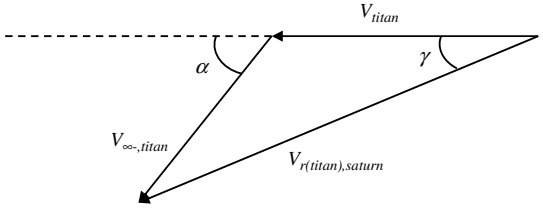

Fig. 3 Titan preflyby (arrival) vector diagram.

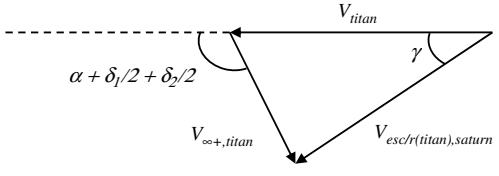

Fig. 4 Titan postflyby (departure) vector diagram.

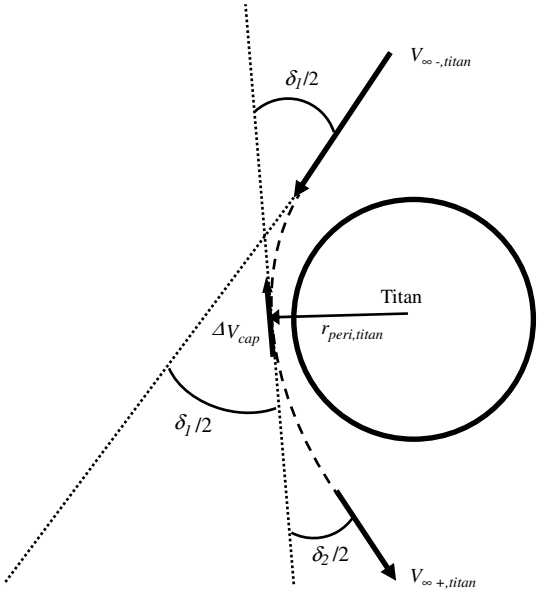

Fig. 5 Schematic of Titan flyby.

$$V_{\infty-,\text{titan}} \sin\alpha = V_{r(\text{titan}),\text{saturn}} \sin\gamma \tag{17}$$

$$\sin(\delta_1/2) = (1 + V^2_{\infty-,\text{titan}} r_{\text{peri,titan}}/\mu_{\text{titan}})^{-1} \tag{18}$$

$$\sin(\delta_2/2) = (1 + V^2_{\infty+,\text{titan}} r_{\text{peri,titan}}/\mu_{\text{titan}})^{-1} \tag{19}$$

We then determine the ΔV_{cap} at Titan needed to achieve parabolic capture at Saturn by subtracting the required periapsis velocity at Titan, $V_{\text{peri}+,\text{titan}}$, from the periapsis velocity at Titan, neglecting atmospheric drag, $V_{\text{peri}-,\text{titan}}$:

$$\Delta V_{\text{cap}} = V_{\text{peri}-,\text{titan}} - V_{\text{peri}+,\text{titan}} \tag{20}$$

where

$$V_{\text{peri}-,\text{titan}} = \sqrt{(2\mu_{\text{titan}}/r_{\text{peri,titan}}) + V^2_{\infty-,\text{titan}}} \tag{21}$$

and

$$V_{\text{peri}+,\text{titan}} = \sqrt{(2\mu_{\text{titan}}/r_{\text{peri,titan}}) + V^2_{\infty+,\text{titan}}} \tag{22}$$

(Note that we assume ΔV_{cap} is instantaneous and that there is no rotation of periapsis during flythrough.) Table 2 shows the results using Eqs. (12–22) with $\gamma = 0$ and 14.5 deg. The case of $\gamma =$ 14.5 deg is the solution for the minimum ΔV_{cap} required at Titan for capture about Saturn, and the $\gamma = 0$ deg case results in the minimum arrival velocity at Titan. Since the ballute mass depends on both the required ΔV_{cap} and the heating rate (which is a function of the cubed velocity), the minimum ΔV_{cap} case may not result in the lowest possible ballute mass. However, the tether mass and propellant masses required for capture are functions of only the velocity change (not the actual speeds) and will therefore be minimized when minimum ΔV_{cap} is minimized.

Table 3 gives the values of the minimum ΔV_{cap}, resulting from Eqs. (11) and (20), at each body.

V. Results

Figures 6 and 7 show the results of several ballute simulations at each planetary body, using both spherical and toroidal ballute configurations. Optimistic (5 W/cm^2) and conservative (2 W/cm^2) heating rate constraints are indicated by the horizontal dashed lines. Points in the lower right-hand side of the figure indicate favorable results with high ballistic coefficient (i.e., small ballutes) and low heating rates. Moving up and to the left-hand side of the figure, the heating rates increase and larger ballutes (i.e., smaller ballistic coefficients) are required to meet the heating constraints. The stagnation-point heating rate is a function of the velocity cubed (with respect to the atmosphere) and the inverse-square of the ballute nose radius. So, in the case of ballutes, dropping into a shallow gravity well (such as Titan's) will mean less mass required for the ballute and conversely dropping into a deep gravity well (such as Jupiter's) results in very high velocities and thus requires greater ballute mass for aerocapture. In fact, because of their large size, the ballutes at Jupiter may be infeasible. The ballute parameters required to meet the conservative 2 W/cm^2 heating constraint, calculated at each body, are given in Table 4.

Compared to the spherical ballute results, the toroidal ballutes require a slightly lower ballistic coefficient (larger ballute area) to achieve the same maximum heating rate. The surface area of a sphere is 4 times its projected frontal area while for the toroid (with a 4:1 radius ratio) it is 3.14 times its projected frontal area. So, less mass is required to build a toroid than a sphere with a given projected frontal area. However, coupled with the toroid's larger drag coefficient but larger heating rate for the smaller curvature (or nose radius), the mass of the ballute material (assuming an equal thickness in all cases) is approximately the same for all of the attractive cases. Interestingly, sometimes the sphere is slightly less massive than the toroid (i.e., at Uranus and Neptune), but sometimes not (i.e., at Venus, Earth, Mars, and Titan). As mentioned earlier, the inflation gas is on the order of a kilogram or less for the attractive cases (with the toroids requiring less gas than the spheres) and would therefore not necessarily tip the balance in favor of one shape verses the other. On the other hand, a toroidal ballute shape may be more attractive than a sphere because the toroid hole will swallow the wake of the leading spacecraft without impinging on the ballute.

Unlike the ballute aerocapture cases, the mass required for propulsive capture and tethered capture does not depend on the heating rate. (In the analysis of the tethered aerocapture system [20], the heating on the tether itself was ignored, though the probe was assumed to have an aeroshell.) Instead, these cases rely directly on the ΔV_{cap} magnitude. So, for both propulsive capture and tethered aerocapture, the higher the ΔV_{cap}, the greater the mass required for capture. For instance, Jupiter has the lowest ΔV_{cap}, namely 0.27 km/s, and hence requires the least propellant mass and the least tether mass for the missions we are considering. For the case at Titan, it is interesting to note that the ballute mass for the minimum ΔV_{cap}

Table 3 Hohmann transfers for minimum ΔV_{cap}

Body	μ, km/s	V_∞, km/s	r_p, km	ΔV_{cap}, km/s
Venus	3.25×10^5	2.71	6190	0.35
Earth	3.99×10^5	2.97	6480	0.39
Mars	4.28×10^4	2.65	3490	0.67
Jupiter	1.27×10^8	5.64	71,900	0.27
Saturn	3.79×10^7	5.44	60,800	0.41
Titan	9.00×10^3	4.00	3080	1.04
Uranus	5.80×10^6	4.66	26,900	0.50
Neptune	6.85×10^6	4.05	25,500	0.34

Table 2 Hohmann transfers for Saturn capture via Titan

Titan	γ, deg	$V_{\infty-,\text{titan}}$, km/s	$V_{\infty+,\text{titan}}$, km/s	α, deg	$\delta_1/2$, deg	$\delta_2/2$, deg	ΔV_{cap}, km/s
Minimum ΔV_{cap}	14.50	4.41	3.17	32.95	7.52	13.04	1.04
Minimum $V_{\infty-,\text{titan}}$	0.00	4.00	2.50	0.00	8.87	18.54	1.20

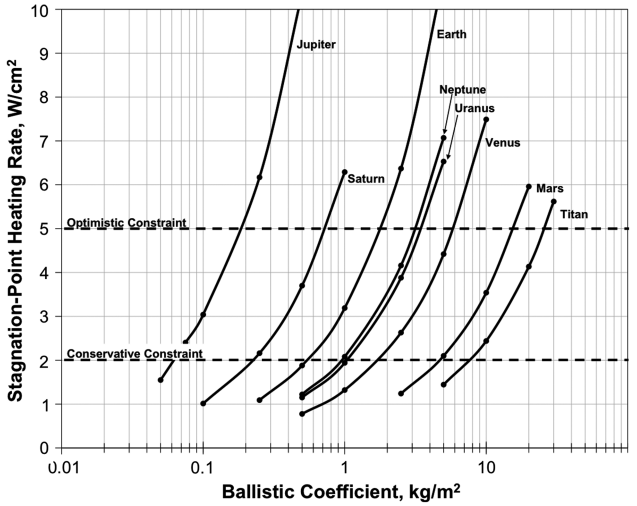

Fig. 6 Maximum stagnation-point heating rates on *spherical* ballutes for a range of sizes.

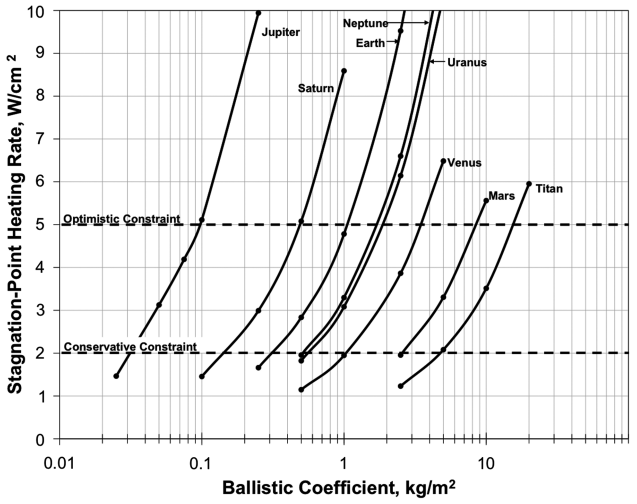

Fig. 7 Maximum stagnation-point heating rates on *toroidal* ballutes for a range of sizes.

case (with $\Delta V_{\text{cap}} = 1.04$ km/s) is greater than that of the minimum $V_{\infty-,\text{titan}}$ case (with $\Delta V_{\text{cap}} = 1.22$ km/s), due to the higher speeds (and therefore higher heating rates) during flythrough.

In Table 5 we compare ballute mass, tether mass, and propellant mass for capture at each of the atmosphere-bearing bodies in the solar system. For the conservative heating constraint of 2 W/cm^2, ballutes are the least massive option for Venus, Mars, Titan, and Uranus; tethers are best (i.e., least massive) at Earth, Jupiter, Saturn, and Neptune. (For the optimistic constraint of 5 W/cm^2, ballutes and tethers are comparable at Earth and Neptune.) Propellant has the highest mass cost in all cases with the exception of Jupiter, where ballutes are the worst, due to Jupiter's deep gravity well.

We now consider the sensitivity of these three capture systems to a small change in the interplanetary trajectory. That is, instead of assuming a Hohmann transfer to Mars, we will consider a more typical scenario in which a more energetic trajectory is used and in which the capture orbit is elliptical (instead of parabolic). We choose a case (from Hall and Le [7]) with an entry velocity of 6.0 km/s (at 125 km altitude), requiring a ΔV_{cap} of 1.69 km/s (much higher than the 0.67 km/s required for the Hohmann transfer case) to target a desired apoapsis altitude of 600 km. A 1000 kg orbiter is again assumed. The results show that a toroidal ballute with a ballistic coefficient of 1.35 kg/m^2 is needed to meet the 2 W/cm^2 heating constraint and capture into the 600 km apoapsis orbit. Similar to the Hohmann transfer case at Mars, the mass for the toroidal ballute (17 kg) is much less (over an order of magnitude less) than the mass of both the tether (715 kg) and propellant (777 kg) required to capture into the 600 km orbit. However, in this instance, the tether mass is comparable to the propellant mass required, while for the Hohmann transfer case, the tether requires less than half of the required propellant mass. So for a 1 km/s increase in ΔV_{cap}, the ballute mass nearly doubles, the propellant mass nearly triples, and the tether mass is over six times greater.

VI. Criticism of the Method

Some questions may arise about the validity of our comparison of the ballute, tether, and propulsion systems in Table 5. For example, the tether spin rate increases the velocity of the probe, which raises its heat-shielding requirements when compared with the orbiter in the propulsive case. On the other hand, the nearly parabolic capture orbit favors the propulsive system, since to get into a more realistic orbit, extra propellant would be required, where the tethered or ballute systems could achieve (at no cost) a lower eccentricity orbit in a second atmospheric pass.

For the tethered system and the propulsive system, no safety factors (such as heating constraints) are taken into account. Although we include heating constraints in the sizing of the ballute system, other issues such as packing and storage, deployment and inflation, determination of the optimal ballute configuration, and coupled aerothermodynamic/structural modeling are ignored in this study. Also, while mass and volume upon arrival at the target body are clearly important, the metrics of injected mass to low-Earth-orbit and injected volume to low-Earth-orbit are crucial. In addition, we have not examined the effects of atmospheric density variations, parameter uncertainties of the system, or guidance and navigation errors for our proposed aerocapture ballute. Tragesser and Longuski [28] have analyzed such stochastic errors affecting the aerocapture tether and have shown that the required tether mass at Mars grows to 368 kg over their deterministic value of 112 kg (shown in Table 5). We do not expect, however, that the ballute mass will increase as dramatically when stochastic errors are taken into account, due to the significant control afforded by the option of severing the ballute once the desired ΔV_{cap} has been achieved.

Table 4 Ballute specifications for a 2 W/cm^2 heating limit

	Spherical Ballute ($C_D = 1$)					Toroidal Ballute ($C_D = 1.37$)					
Body	R_{sball}, m	A_{sball}, m^2	S_{sball}, m^2	m_{ball}, kg	β, kg/m^2	R_{tball}, m	r_{tball}, m	A_{tball}, m^2	S_{tball}, m^2	m_{ball}, kg	β, kg/m^2
Venus	13.7	588	2350	23.4	1.74	15.1	3.80	718	2250	22.4	1.04
Earth	25.2	2000	8000	79.5	0.54	28.0	7.00	2460	7720	76.7	0.32
Mars	8.30	216	862	8.60	4.68	9.5	2.40	285	897	8.90	2.58
Jupiter	125	49,400	198,000	1960	0.06	180	44.9	101,000	318,000	3160	0.03
Saturn	40.9	5260	21,000	209	0.23	42.7	10.7	5740	18,000	179	0.15
Titan (min ΔV_{cap})	6.40	129	515	5.12	7.80	7.00	1.75	154	484	4.81	4.76
Titan (min $V_{\infty-,\text{titan}}$)	5.81	106	424	4.21	9.48	6.30	1.57	124	391	3.88	5.89
Uranus	17.8	1000	4000	39.8	1.04	20.6	5.20	1330	4190	41.7	0.57
Neptune	18.7	1100	4390	43.7	0.95	21.6	5.40	1470	4610	45.8	0.52

Table 5 Aerocapture results for solar system exploration

Body	ΔV, km/s	Ballute mass (sphere), kg	Ballute mass (toroid), kg	Propellant mass (Δm), kg	Tether mass, kg
Venus	0.35	23	22	126	31
Earth	0.39	79	77	142	38
Mars	0.67	9	9	256	112
Jupiter	0.27	1960	3160	96	18
Saturn	0.41	209	179	149	42
Titan (min ΔV_{cap})	1.04	5	5	425	271
Titan (min $V_{\infty-,\text{titan}}$)	1.20	4	4	502	358
Uranus	0.50	40	42	185	63
Neptune	0.34	44	46	122	29

The ballute mass versus tether mass versus propellant mass study is chosen as a simple way to evaluate the performance of the ballute system. The favorable results presented in this analysis indicate that a more detailed examination may prove fruitful.

VII. Conclusions

Ballutes can be used to achieve aerocapture while maintaining low thermal loads. Because of the large radii (tens of meters) of such ballutes, aerocapture can occur at such high altitudes that the temperature of the proposed ballute material (Kapton) does not exceed 500°C. In spite of their large size, aerocapture ballutes can have low masses, due to the extremely thin layer of Kapton required (about 7 μm). Aerocapture ballutes represent an emerging technology that can significantly reduce the fractional thermal protection mass required for achieving capture into orbit about many of the atmosphere-bearing bodies in the solar system. Another proposed technology in the literature is the aerocapture tether, which has the potential (according to feasibility studies) to be significantly less massive than the propellant required for capture.

In this paper, we considered capture at Venus, Earth, Mars, Jupiter, Saturn, Titan, Uranus, and Neptune. We have analyzed propellant cost and compared those costs to the masses of the aerocapture tethers and aerocapture ballutes. Based on the mass comparison (lower masses being better than higher masses), ballutes offer the best performance option for capture at Venus, Mars, Titan, and Uranus, and the worst performance option for capture at Jupiter. Tethers are the best option for capture at Earth, Jupiter, Saturn, and Neptune. Chemical-propulsion capture provides the worst performance option everywhere except at Jupiter (where the ballute is the worst). The results indicate that the advantages of ballutes should be studied in greater detail with assessments of the other necessary hardware (e.g., deployment and inflation mechanisms). For ballute applications, the low system mass for Venus, Mars, and Titan appear feasible and attractive for early missions.

Acknowledgments

This work was sponsored in part by a NASA Graduate Student Research Program (GSRP) fellowship from Marshall Space Flight Center (MSFC), under contract number NNM05ZA11H, and by the Jet Propulsion Laboratory (JPL), California Institute of Technology. We would like to thank the former In-Space Propulsion Team for their support, especially Bonnie F. James (GSRP Technical Advisor) of MSFC and Michelle M. Munk and Erin H. Richardson of NASA Langley Research Center. Also, we are grateful to Angus D. McRonald (of Global Aerospace Corporation) and Daniel T. Lyons (of JPL) for their valuable assistance and advice.

References

[1] McRonald, A. D., "A Light-Weight Inflatable Hypersonic Drag Device for Planetary Entry," *Association Aeronautique de France Conference*, Arcachon France, 16–18 March 1999.

[2] McRonald, A. D., "A Light-Weight Inflatable Hypersonic Drag Device for Venus Entry," American Astronautical Society Paper 99-355, Aug. 1999.

[3] McRonald, A. D., "A Light-Weight Hypersonic Inflatable Drag Device for a Neptune Orbiter," American Astronautical Society Paper 00-170, Jan. 2000.

[4] Turk, R. A., "Pressure Measurements on Rigid Model of Ballute Decelerator at Mach Numbers from 0.56 to 1.96," NASA TN D-3545, 1966.

[5] Jaremenko, I. M., "Ballute Characteristics in the 0.1 to 10 Mach Number Speed Regime," *Journal of Spacecraft and Rockets*, Vol. 4, No. 8, 1967, pp. 1058–1063. doi:10.2514/3.29018

[6] Park, C., "Theory of Idealized Two-Dimensional Ballute in Newtonian Hypersonic Flow," *Journal of Spacecraft and Rockets*, Vol. 25, No. 3, May–June 1988, pp. 217–224. doi:10.2514/3.25974

[7] Hall, J. L., and Le, A. K., "Aerocapture Trajectories for Spacecraft with Large, Towed Ballutes," American Astronautical Society Paper 01-235, Feb. 2001.

[8] Westhelle, C. H., and Masciarelli, J. P., "Assessment of Aerocapture Flight at Titan Using a Drag-only Device," AIAA Paper 2003-5389, Aug. 2003.

[9] Lyons, D. T., and McRonald, A. D., "Entry, Descent and Landing Using Ballutes," *2nd International Planetary Probe Workshop*, NASA Ames Research Center, Moffet Field, CA, Aug. 2004.

[10] Johnson, W. R., and Lyons, D. T., "Titan Ballute Aerocapture Using a Perturbed TitanGRAM Model," AIAA Paper 2004-5280, Aug. 2004.

[11] Lyons, D. T., and Johnson, W. R., "Ballute Aerocapture Trajectories at Neptune," AIAA Paper 2004-5181, Aug. 2004.

[12] Lyons, D. T., and Johnson, W. R., "Ballute Aerocapture Trajectories at Titan," *Advances in the Astronautical Sciences*, Vol. 116, edited by J. de Lafontain, A. J. Treder, M. T. Soyka, and J. A. Sims, Univelt, San Diego, CA, 2004, pp. 2275–2294; also American Astronautical Society, Paper AAS 03-646.

[13] Gates Medlock, K. L., Longuski, J. M., and Lyons, D. T., "A Dual-Use Ballute for Entry and Descent During Planetary Missions," *3rd International Planetary Probe Workshop*, Attica, Greece, 27 June–1 July 2005.

[14] Gates Medlock, K. L., and Longuski, J. M., "An Approach to Sizing a Dual-Use Ballute System for Aerocapture, Descent and Landing," *4th International Planetary Probe Workshop*, Pasadena, CA, 27–30 June 2006.

[15] Miller, K. L., Gulick, D., Lewis, J., Trochman, B., Stein, J., Lyons, D. T., and Wilmoth, R., "Trailing Ballute Aerocapture: Concept and Feasibility Assessment," AIAA Paper 2003-4655, July 2003.

[16] Richardson, E. H., Munk, M. M., James, B. F., and Moon, S. A., "Review of NASA In-Space Propulsion Technology Program Inflatable Decelerator Investments," AIAA Paper 2005-1603, May 2005.

[17] Masciarelli, J. P., Lin, J. K. H., Ware, J. S., Rohrschneider, R. R., Braun, R. D., Bartels, R. E., Moses, R. W., and Hall, J. L., "Ultra Lightweight Ballutes for Return to Earth from the Moon," AIAA Paper 2006-1698, May 2006.

[18] Rohrschneider, R. R., and Braun, R. D., "Survey of Ballute Technology for Aerocapture," *Journal of Spacecraft and Rockets*, Vol. 44, No. 1, Jan.–Feb. 2007, pp. 10–23. doi:10.2514/1.19288

[19] Puig-Suari, J., and Longuski, J. M., "Perturbation Analysis of Aerocapture with Tethers," American Astronautical Society Paper 91-549, Aug. 1991.

[20] Longuski, J. M., Puig-Suari, J., and Mechalas, J., "Aerobraking Tethers for the Exploration of the Solar System," *Acta Astronautica*, Vol. 35, Nos. 2/3, 1995, pp. 205–214. doi:10.1016/0094-5765(94)00273-O

[21] Longuski, J. M., Puig-Suari, J., Tsiotras, P., and Tragesser, S., "Optimal Mass for Aerobraking Tethers," *Acta Astronautica*, Vol. 35, No. 8, 1995, pp. 489–500.

doi:10.1016/0094-5765(95)00006-L
[22] Gates, K. L., McRonald, A. D., and Nock, K. T., "HyperPASS, a New Aeroassist Tool," *2nd International Planetary Probe Workshop*, NASA Ames Research Center, Moffet Field, CA, Aug. 2004.
[23] Sutton, K., and Graves, R. A., Jr., "A General Stagnation Point Convective Heating Equation for Arbitrary Gas Mixtures," NASA Langley Research Center TR R-376, Hampton, VA, Nov. 1971.
[24] Gnoffo, P. A., and Anderson, B. P., "Computational Analysis of Towed Ballute Interactions," AIAA Paper 2002-2997, June 24–26, 2002.
[25] Cox, R. N., and Crabtree, L. F., *Elements of Hypersonic Aerodynamics*, Academic Press, New York, 1965.
[26] Moss, J., "DSMC Simulations of Ballute Aerothermodynamics Under Hypersonic Rarefied Conditions," AIAA Paper 2005-4949, June 2005.
[27] Gnoffo, P., Buck, G., Moss, J., Nielsen, E., Berger, K., Jones, W. T., and Rudavsky, R., "Aerothermodynamic Analyses of Towed Ballutes," AIAA Paper 2006-3771, June 2006.
[28] Tragesser, S. G., and Longuski, J. M., "Analysis and Design of Aerocapture Tether with Accounting for Stochastic Errors," *Journal of Spacecraft and Rockets*, Vol. 35, No. 5, 1998, pp. 683–689. doi:10.2514/2.3385

C. Kluever
Associate Editor